

## Determination of Surface-Defect Concentration and Distribution with He Diffraction

W. A. Schlup and K. H. Rieder

IBM Zurich Research Laboratory, 8803 Rüschlikon, Switzerland

(Received 14 June 1985)

A pronounced triangular background, observed near the specular beam with He diffraction from Ni(100)- $c(2 \times 2)O$ , is explained by hard-wall calculations as originating from a random distribution of  $\approx 15\%$  empty oxygen sites in good agreement with Auger calibration. Lateral adatom relaxations of  $\approx 0.25 \text{ \AA}$  away from the empty sites fit both the background shape and intensity. This is the first application of He scattering for defect characterization at high coverages.

PACS numbers: 68.35.Dv, 61.16.Fk

Diffraction experiments can give information not only on the regular arrangement of the scatterers but also on deviations from order; the first is contained in the intensity of the Bragg peaks, and the second in the shape and intensity of the diffuse background scattering.<sup>1</sup>

Analyses of He-beam diffraction intensities yield the corrugation function, which is a replica of the surface electron-density contour,<sup>2</sup> and often shows the location of the surface atoms relative to one another in a direct manner. This is actually the case for the  $p(2 \times 2)$  and  $c(2 \times 2)$  phases of oxygen on Ni(100): In both phases, the adsorbates form pronounced hills with the same height and very similar shape on the essentially flat basic corrugation of the substrate, indicating identical geometrical and similar electronic states of the oxygen adatoms in both phases.<sup>3</sup> These conclusions were confirmed by numerous independent investigations with different methods.<sup>4-6</sup>

Whereas the widths of the diffraction peaks of the  $p(2 \times 2)$  phase were in accordance with the angular and velocity spread of the incoming beam, and no structure was observed between the Bragg beams,<sup>3</sup> all in-plane diffraction scans even of the best ordered  $c(2 \times 2)$  showed a pronounced nearly triangular background around the specular as can be seen from Fig. 1; in this configuration the beam impinges along the diagonal of the  $c(2 \times 2)$  primitive cell ( $\alpha = 45^\circ$ , inset in Fig. 2). Diffraction scans with the beam incident along one of the unit-cell vectors of the  $c(2 \times 2)$  ( $\alpha = 0^\circ$ ) exhibited a very similar triangular shape around the specular so that the total diffuse-scattering contribution appears cone-shaped. The broad small structure in the out-of-plane scan at  $\psi = \pm 6.6^\circ$  between the beams  $(\bar{1}0)$  and  $(01)$  also arises from this background structure. That this background is mainly due to static disorder was strongly suggested by diffraction scans at different temperatures which showed that the intensity ratios between the Bragg peaks and the background structure remained essentially unchanged. A first hint as to the origin of this background was obtained by measurements of oxygen Auger intensities in both phases: When we fix the

coverage of the (obviously better ordered)  $p(2 \times 2)$  at the ideal value of 0.25 monolayer (ML), the intensity ratio yielded for the  $c(2 \times 2)$  coverage values  $\approx 15\%$  smaller than the ideal 0.5 ML in accordance with simi-

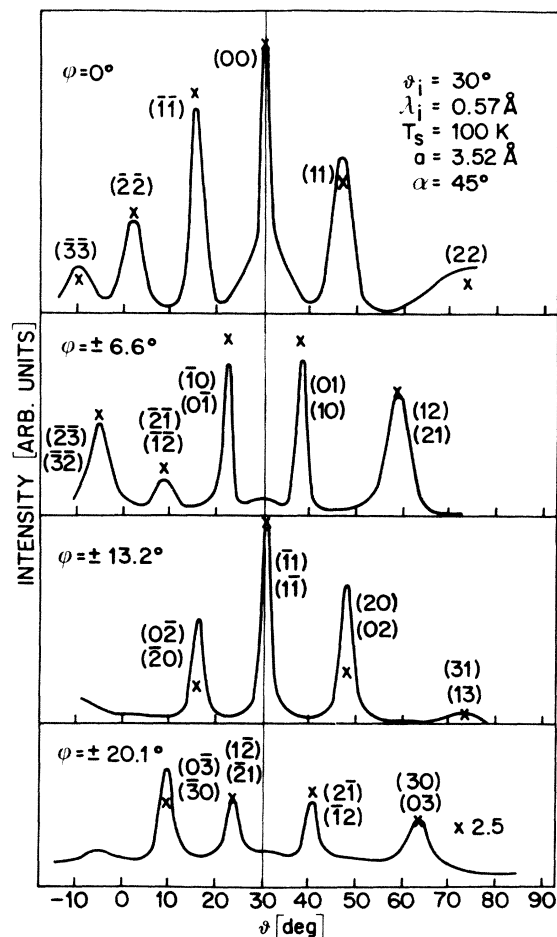


FIG. 1. Typical in-plane and out-of-plane He-diffraction spectra for the  $c(2 \times 2)$  phase of oxygen on Ni(100). The diffraction peaks are indexed according to the unit cell of the adsorbate structure ( $a = 3.52 \text{ \AA}$ ). The best-fit peak intensities obtained with the simplified corrugation model are indicated as crosses.

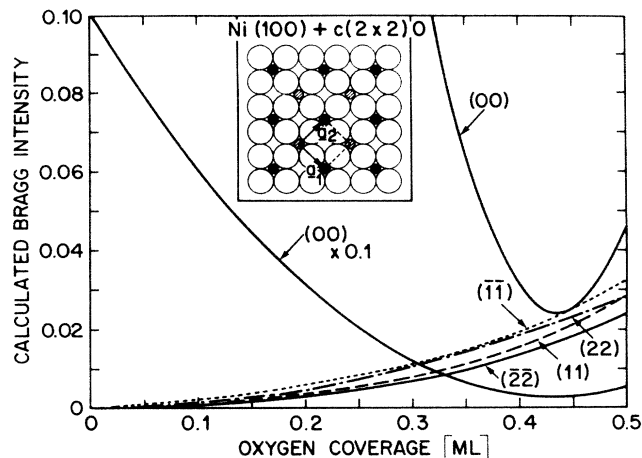


FIG. 2. Calculated diffraction-beam intensities for increasing coverage. The best-fit hard-wall corrugation parameters describing individual oxygen hills on the flat Ni(100) substrate are used. Note the smooth decrease of the specular and the smooth increase of the diffraction beams with increasing coverage. In real cases, the intensity at very low coverages decreases much more rapidly because of the giant cross section of isolated adatoms (Ref. 11). The experimental intensity merges into the hard-wall curve at high coverages. The inset shows a model of the  $c(2 \times 2)$  oxygen phase on Ni(100); large open circles denote Ni atoms, and small full and hatched circles distinguish the two different oxygen sublattices discussed in the text.

lar observations in many other investigations of this system.<sup>7</sup>

Our model calculations on the diffraction from surfaces with defects confirmed the above amount of oxygen defect concentrations, and showed that the unoccupied sites are essentially randomly distributed and that a lateral relaxation of the surrounding adsorbate atoms away from the empty sites very likely takes place. A distribution in which the  $p(2 \times 2)$  sites are all occupied and only the  $c(2 \times 2)$  sites are amenable to random occupation, which also appears possible because of formation of the  $c(2 \times 2)$  out of the  $p(2 \times 2)$ , could be definitely excluded.

We start with the best-fit analyses of the measured Bragg intensities, wherein for the specular only the intensity without the triangular background was taken. The best-fit calculations were performed on the basis of the hard corrugated-wall model with the eikonal approximation by assumption of a completely flat substrate corrugation and by a modeling of the individual oxygen adatoms as generalized Gaussian hills of the form

$$H \exp\{-[\ln 2 / (\frac{1}{2}B)^S][(x-x_0)^S + (y-y_0)^S]\};$$

$H$  denotes the height, and  $B$  the full width at half maximum; variation of  $S$  allows slight variation of the shape and symmetry of the hills. The surface unit-cell

length of the  $c(2 \times 2)$  phase is  $a = 3.52 \text{ \AA}$ . The best-fit diffraction peak intensities are shown as crosses in Fig. 1. The proper broadening of the beams due to the finite angular divergence and the velocity spread of the incoming beam has been taken into account. The best-fit parameters for this particular spectrum are  $H = 0.61 \text{ \AA}$ ,  $B = 2.09 \text{ \AA}$ , and  $S = 2.2$  in very good agreement with the parameters reported earlier.<sup>3</sup> A somewhat better fit of the higher-order out-of-plane beams can be obtained by taking also the amplitude of the basic corrugation of the substrate as a free parameter, but this plays a negligible role in connection with the defect problem. The fact that  $S > 2$  is required in our simplified model is in accordance with the observation of charge-density bridges between nearest-neighbor adatoms in the  $c(2 \times 2)$  as previously pointed out in connection with the Fourier analysis of the corrugation.<sup>3</sup>

To investigate the origin of the diffuse scattering around the specular, we performed calculations for different surface concentrations by considering for each coverage several hundred randomly chosen adsorbate site configurations on  $N \times N$  meshes of the  $c(2 \times 2)$  unit cell ( $N = 8-12$ ) and averaging over all calculated intensity distributions. The validity of the eikonal approach, which works very well for integration over a single unit cell, was proven for the  $N \times N$  meshes by reproduction of the Bragg intensities with all lattice sites occupied. Because of the flatness of the basic corrugation, for zero adatom concentration the whole diffracted intensity goes into the specular beam, Fig. 2. If we assume uncorrelated random occupation of the  $N \times N$  available sites for all coverages  $0 \leq \theta \leq 0.5 \text{ ML}$ , the specular intensity initially drops, goes through a minimum at a coverage of  $\approx 0.43 \text{ ML}$ , and increases slightly when approaching saturation; the diffraction peaks exhibit a continuous increase with increasing coverage (Fig. 2). The intensity behavior goes exactly quadratic with coverage as long as the individual adatom corrugations do not overlap.<sup>8</sup> Deviation from this parabolic behavior in the present case is due to the overlapping adatom hills which form bridges<sup>3</sup> between nearest-neighbor adatoms since  $S > 2$ . Figure 3(b) shows the in-plane intensity distribution for a coverage of  $0.43 \text{ ML}$  which corresponds to the minimum specular intensity. The calculated distribution clearly shows a background around the specular whose shape closely resembles that of the experiment. These results compare very well with those of model calculations of atomic-beam scattering from imperfect surfaces performed with other methods.<sup>8-10</sup> Figure 2 strongly suggests that the defect concentration in the  $c(2 \times 2)$ O phase has to be around 15% of the saturation value of  $0.5 \text{ ML}$ , since at lower coverages the specular would be overestimated, and at higher coverages the background around the specular would be even smaller. It

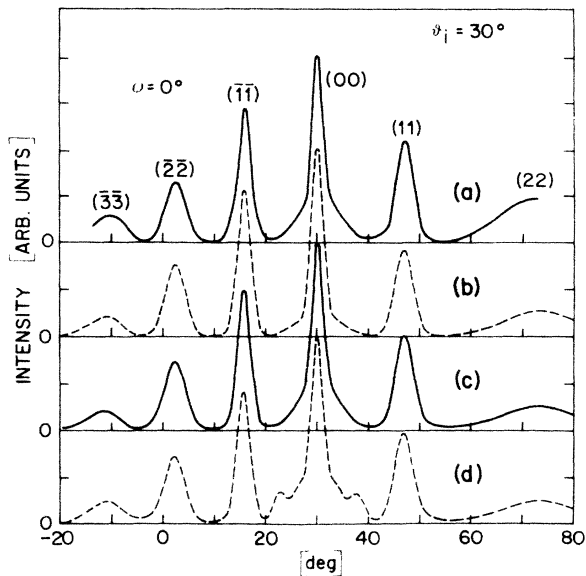


FIG. 3. (a) Experimental in-plane intensity scan of Fig. 1. (b) Calculated intensity distribution for a random distribution of  $\approx 15\%$  oxygen vacancies (coverage 0.43 ML); note that in this case the triangular background is too small as compared to experiment. (c) Calculated intensity distribution for the same oxygen coverage but with a lateral relaxation of the adatoms of  $\approx 0.25$  Å away from the empty sites; the background around the specular is quantitatively reproduced. (d) A defect distribution in which the  $p(2 \times 2)$  sites (black circles in Fig. 2) are frozen in, and the disorder restricted to the  $c(2 \times 2)$  sites (hatched circles in Fig. 2) does not reproduce experiment.

is quite satisfactory that our analysis of the He-scattering data does indeed require the defect concentration to be close to the value obtained with the Auger measurements. The intensity of the calculated background is, however, too small relative to the diffraction beams.

With the coverage fixed at 0.43 ML, we therefore investigated how the background around the specular is influenced by lateral relaxations of the adatoms away from or towards the unoccupied sites. We found that only relaxation away from the empty sites increases the background without essentially changing its triangular shape. Optimum agreement with experiment was obtained for a lateral relaxation of  $\approx 0.25$  Å; in this case also the small structure in the first out-of-plane scans between the  $(\bar{1}0)$  and  $(01)$  beams could be reproduced. Lateral relaxation towards the unoccupied sites introduces structure in the background around the specular and also between higher-order diffraction beams which is clearly not observed experimentally. We may speculate that the formation of bridges between nearest-neighbor oxygen adatoms observed in the charge-density contours of the  $c(2 \times 2)$  signals attractive interaction between the adatoms, so that relax-

ation away from unoccupied sites would be a natural consequence.

According to the fact that the  $c(2 \times 2)$  phase grows out of the  $p(2 \times 2)$  with the ideal coverage of 0.25 ML upon further oxygen exposure, it could be conceived that the  $p(2 \times 2)$  sublattice sites (black circles in the inset of Fig. 2) remain fixed and that disorder is restricted to the other sublattice which becomes occupied by the formation of the  $c(2 \times 2)$  phase (hatched circles in inset of Fig. 2). However, this is not the case as can be seen from Fig. 3(d), which was obtained under this assumption [lateral relaxation of 0.25 Å away from the empty sites is taken into account in Fig. 3(d)]. The broad peaklike structures between the  $c(2 \times 2)$  Bragg reflections can be regarded as remnants of Bragg peaks of the  $p(2 \times 2)$  phase. The fact that no such structure is observed in the various diffraction scans shows that upon formation of the  $c(2 \times 2)$ , the  $p(2 \times 2)$  sites are not frozen in, but that all sites in both sublattices are statistically equivalent. This seems reasonable in view of the fact that adsorption was performed at a surface temperature of 600 K, which ensures sufficient mobility of the adatoms, and that the sample was rapidly cooled for the diffraction experiments to 100 K, where the adatoms are practically immobile. Extended calculations considering line defects, which were created by isotropic random walks both to nearest and next-nearest-neighbor sites, never reproduced the triangular background experimentally observed. Influence of antiphase domains can also be excluded since no splitting of Bragg beams is observed.

Atomic-beam scattering from a surface with a high density of adsorbates is qualitatively different from that at very low coverages, investigated<sup>11</sup> and applied<sup>12</sup> by Poelsema, Verheij, and Comsa. In the first case, the scattering distribution is determined by the hard-wall repulsive potential since the attractive part is homogeneous and not influenced greatly by single missing adatoms in a dense overlayer.<sup>13</sup> At low coverages, on the other hand, single adatoms create an attractive aureole around their adsorption sites<sup>11,13</sup> which gives rise to a "giant cross section" due to different refraction of the atoms on their ways to and from the surface<sup>12</sup> in the vicinity of the adsorbates. As a result of this effect, a much stronger intensity drop is observed at very low coverages than that obtained with the hard-wall calculations; the real curve merges into the hard-wall behavior at higher coverages.<sup>13,14</sup>

Our model calculations with random hollow sites also reproduced the experimental observation that the triangular background is the more pronounced the smaller  $\theta_i$ . Calculations for diffraction data obtained for  $\theta_i = 40^\circ$  (see Fig. 2 in Ref. 3) confirmed the above conclusions on defect concentration and distribution. Nevertheless, it would be extremely valuable for the further development of the field of He diffraction

from surfaces with defects to obtain confirmation of our present results with a real-space method like the scanning tunneling microscope. We note in closing that the appreciable amount of oxygen defects in the  $c(2 \times 2)$  phase may be the reason for the strong Debye-Waller factor observed in LEED,<sup>15</sup> because of the possibility of low-lying defect modes.

The authors thank W. Stocker for his skillful assistance during the experiments, and E. Courtens and E. Tosatti for discussions.

---

<sup>1</sup>J. M. Cowley, *Diffraction Physics* (North-Holland, Amsterdam, 1984).

<sup>2</sup>N. Esbjerg and J. K. Norskov, *Phys. Rev. Lett.* **45**, 807 (1980); J. Harris and A. Liebsch, *J. Phys. C* **15**, 2275 (1982).

<sup>3</sup>K. H. Rieder, *Phys. Rev. B* **27**, 6978 (1983), and *Surf. Sci.* **128**, 325 (1983).

<sup>4</sup>J. Stoehr, R. Jaeger, and T. Kendelewitz, *Phys. Rev. Lett.* **49**, 142 (1982).

<sup>5</sup>C. W. Bauschlicher, S. P. Walch, P. S. Bagus, and C. R.

Brundle, *Phys. Rev. Lett.* **50**, 864 (1983); C. W. Bauschlicher and C. R. Brundle, *Phys. Rev. Lett.* **52**, 200 (1984), and **54**, 349 (1985).

<sup>6</sup>M. De Crescenci, F. Antonangeli, C. Bellini, and R. Rossi, *Phys. Rev. Lett.* **50**, 1949 (1983).

<sup>7</sup>For a recent review, see C. R. Brundle and J. Q. Broughton, IBM Research Report No. RJ 4499, 1984 (unpublished).

<sup>8</sup>A. C. Levi, R. Spadacini, and G. E. Tommei, *Surf. Sci.* **108**, 181 (1981); A. C. Levi, *Surf. Sci.* **121**, 504 (1982).

<sup>9</sup>G. Drolshagen and E. J. Heller, *J. Chem. Phys.* **79**, 2072 (1983).

<sup>10</sup>R. B. Gerber, A. T. Yinnon, and R. Kosloff, *Chem. Phys. Lett.* **105**, 523 (1984).

<sup>11</sup>B. Poelsema, S. T. de Zwart, and G. Comsa, *Phys. Rev. Lett.* **49**, 578 (1982), and **51**, 522(E) (1983); B. Poelsema, R. L. Palmer, S. T. de Zwart, and G. Comsa, *Surf. Sci.* **126**, 641 (1983).

<sup>12</sup>B. Poelsema, L. K. Verheij, and G. Comsa, *Phys. Rev. Lett.* **49**, 1731 (1982), and **51**, 2410 (1983).

<sup>13</sup>E. Zaremba, *Surf. Sci.* **151**, 91 (1985).

<sup>14</sup>H. Wilsch and K. H. Rieder, *J. Chem. Phys.* **78**, 7491 (1983).

<sup>15</sup>J. E. Demuth, N. J. DiNardo, and G. S. Cargill, III, *Phys. Rev. Lett.* **50**, 1373 (1983).